Rotational dynamics of rigid, symmetric top macromolecules. Application to circular cylinders

María M. Tirado and José García de la Torre

Citation: The Journal of Chemical Physics **73**, 1986 (1980); doi: 10.1063/1.440288
View online: http://dx.doi.org/10.1063/1.440288
View Table of Contents: http://aip.scitation.org/toc/jcp/73/4
Published by the American Institute of Physics

Rotational dynamics of rigid, symmetric top macromolecules. Application to circular cylinders

María M. Tirado and José García de la Torre

Departamento de Química Física, Facultad de Ciencias, Universidad de Extremadura, Badajoz, Spain
(Received 21 April 1980; accepted 2 May 1980)

The formalism for the calculation of translational friction coefficients of symmetric top macromolecules presented in a previous paper [M. M. Tirado and J. García de la Torre, *J. Chem. Phys.* **71**, 2585 (1979)] is here extended to the evaluation of rotational friction and diffusion coefficients. We show how the introduction of symmetry considerations leads to a great reduction of the computational requirements needed to solve the hydrodynamic interaction equations. We also obtain the translation–rotation coupling tensor from which the center of hydrodynamic stress can be obtained. For a rigid ring we have derived analytical solutions that reduce to those obtained by other authors when the unmodified interaction tensor is used. The general formalism is finally applied to the calculation of the rotational diffusion coefficients of circular cylinders modeled as stacks of rings and extrapolated to zero bead size. The resulting values are critically compared with those from earlier studies.

I. INTRODUCTION

In a previous paper,[1] which will be hereafter referred to as Paper I, we considered the calculation of the translational friction tensor of rigid symmetric top macromolecules. The symmetry elements that characterize this kind of particle, namely, an axis of symmetry plus a symmetry plane containing the axis, were taken into account to devise a modified method which is far more efficient than the standard one[2–6] in regard to computer requirements. Thus, we were able to calculate friction coefficients of models composed of a very large number of frictional elements, near the ideal shell-model limit.[7]

In this paper we present a similar treatment for the rotational coefficients of rigid symmetric top macromolecules. Rotation is considered around both the symmetry axis and any axis perpendicular to it. In the latter case, obtaining of the center of hydrodynamic stress[8,9] is necessary, and is accomplished with full inclusion of hydrodynamic interaction by using results of previous work.[10,11]

The rotation about a perpendicular axis had been studied earlier[12–15] in a one dimensional scheme, by assuming that the frictional forces were in the same direction as the unperturbed linear velocities. Although this is only true for some particular instances,[16] generalization to other cases was made in order to achieve a notable simplification in the computational procedures that made it possible the calculation for complex models of T-even phage.[13] Here we discuss this approach by looking at the approximations that are involved in it and comparing its results with those from the rigorous treatment.

The major application of the method for translation in Paper I was to obtain the translational friction coefficients of rigid cylinders, and two important conclusions were drawn. First, the effect of the end plates was shown to be negligible. Second, our results along with those from many other studies were in remarkable disagreement with Broersma's theory.[17] An independent work by Norisuye *et al.*[18] seems to confirm both facts. In this paper we shall carry out a similar application to calculate the rotational friction coefficients of cylinders over a wide range of the length-to-diameter ratios, and the results will be critically compared with those predicted by other authors.

II. THEORY

A. Generalities

Throughout this paper we use the definitions and notation introduced in Paper I. Let us choose a system of Cartesian coordinates (x_1, x_2, x_3) in such a way that x_3 is the symmetry axis. No restriction is placed on x_1 and x_2. The center of coordinates is an arbitrary point O. For each bead cylindrical coordinates (θ_i, r_i, z_i), $i = 1, \ldots, N$, are defined,[1] with $z \equiv x_3$. The N beads composing the model are considered as a set of N_r rings. The kth ring has n_k beads, with $n_k = s$, s being the symmetry number, or $n_k = 1$ when the ring just consists of a bead lying on the z axis. Thus, each ring is characterized by θ_k, r_k, z_k, where $\theta_k = \min(\theta_i)$, $i \in k$.

As z coincides with the axis of symmetry, the translational friction tensor Ξ_t, and the rotational friction tensor at any point P, $\Xi_{P,r}$ are diagonal[8] with two equal components $\Xi_t^{11} = \Xi_t^{22}$ and $\Xi_{P,r}^{11} = \Xi_{P,r}^{22}$. $\Xi_{P,r}^{33}$ corresponds to rotation around the axis of symmetry and obviously does not depend on the choice of P. However, $\Xi_{P,r}^{11}$ for a perpendicular axis, does depend on P. The third fundamental tensor for characterizing the Brownian dynamics of the particle is the translation–rotation coupling tensor[3,8,10] $\Xi_{P,c}$, which is also origin dependent. For symmetric tops, $\Xi_{R,c} = 0$ when referred to R, the center of hydrodynamic stress.[8] Then the translational and rotational diffusion tensors $\mathbf{D}_t$ and $\mathbf{D}_r$ are given by

$$\mathbf{D}_t = k_B T \Xi_t^{-1} , \tag{1}$$

$$\mathbf{D}_r = k_B T \Xi_{R,r}^{-1} . \tag{2}$$

Here k_B is Boltzmann's constant and T is the absolute temperature {not to be confused with interaction tensors [Eq. (4)] or torques [Eq. (27)]}. When the particle has in addition a center of symmetry, it coincides with R; such is the case for cylinders. Otherwise R has to be calculated from the translation and coupling tensors.

 0021-9606/80/161986-08$01.00

For symmetric tops, an especially simple relation holds[8,10]

$$z_{OR} = -\Xi^{12}_{O,c}/\Xi^{11}_{t} , \tag{3}$$

where z_{OR} is the distance between R and the origin of coordinates along the z axis.

B. Rotation around the symmetry axis Ξ^{33}_r

The hydrodynamic interaction equation in cylindrical coordinates is given by Eq. (I.13) (I denotes Paper I):

$$\mathbf{F}^c_i + \sum_{j=1}^{N}{}' \zeta_i \mathbf{T}^c_{ij} \cdot \mathbf{F}^c_j = \zeta_i \mathbf{u}^c_i , \quad i = 1, \ldots, N . \tag{4}$$

ζ_i, $\mathbf{u}^c_i$, and $\mathbf{F}^c_i$ are, respectively, the Stokes-law frictional coefficient of bead i, $6\pi\eta_0\sigma_i$, and the cylindrical components of the unperturbed velocities and frictional forces. The T^c_{ij} are the modified interaction tensors in cylindrical coordinates, Eqs. (I.A1–I.A12) in Paper I.

When the particle is rotating around its symmetry axis with angular velocity ω, the unperturbed velocity of the ith bead is

$$\mathbf{u}^c_i = (\omega r_i , 0, 0)^T , \tag{5}$$

the r and z components being zero. Then, by performing Jacobi iterations on Eq. (4) it is easily shown that the forces have the same form, i.e.,

$$\mathbf{F}^c_i = (F^\theta_i , 0, 0)^T , \tag{6}$$

and therefore Eq. (4) reduces to a scalar equation

$$F^\theta_i + \zeta_i \sum_j{}' T^{\theta\theta}_{ij} F^\theta_j = \zeta_i \omega r_i . \tag{7}$$

Now we define

$$C_i = F^\theta_i / \omega r_i \zeta_i . \tag{8}$$

Note that C_i behaves like a shielding coefficient ($C_i \to 1$ for weak interaction, $C_i \to 0$ for strong interaction). From Eqs. (7) and (8) we get

$$C_i + \sum_j{}' \zeta_i T^{\theta\theta}_{ij} r_i^{-1} r_j C_j = 1 . \tag{9}$$

In the present case the velocity field has the same symmetry as the particle. Hence, the forces (θ components) must be identical for all the beads in a given ring, i.e., $F^\theta_i \equiv F^\theta_k$, $i \in k$, or $C_i \equiv C_k$ since $r_i \equiv r_k$ and $\zeta_i \equiv \zeta_k$. Moreover, the sum in Eq. (9) can be decomposed as follows[1]:

$$\sum_j{}' = \sum_{\substack{j \in k \\ j \neq i}}^{n_k} + \sum_{\substack{l=1 \\ l \neq k}}^{N_r}{}' \sum_{j \in l}^{n_l} . \tag{10}$$

Thus, Eq. (9) now reads

$$\sum_{l=1}^{N_r} B_{kl} C_l = 1 , \quad k = 1, \ldots, N_r , \tag{11}$$

where

$$B_{kl} = \delta_{kl}\left(1 + \sum_{j \in k}{}' \zeta_j T^{\theta\theta}_{ij}\right) + (1 - \delta_{kl}) r_k r_l^{-1} \sum_{j \in l} \zeta_j T^{\theta\theta}_{ij} . \tag{12}$$

The total torque on the particle is given by

$$T = \sum_{i=1}^{N} r_i F^\theta_i = \sum_{i=1}^{N} \omega C_i (r_i)^2 \zeta_i = \Xi^{33}_r \omega . \tag{13}$$

Therefore,

$$\Xi^{33}_r = \sum_{i=1}^{N} C_i (r_i)^2 \zeta_i = \sum_{k=1}^{N_r} n_k C_k (r_k)^2 \zeta_k . \tag{14}$$

The evaluation of Ξ^{33}_r requires the solution of a system of linear equations, Eq. (11), whose $N_r \times N_r$ matrix of coefficients can be obtained from the geometry of the model via Eq. (I.A1).

C. Location of the center of hydrodynamic stress

In contrast to Ξ^{33}_r, the rotational friction coefficient for any perpendicular axis is origin-dependent, and the values to be substituted in Eq. (2) are precisely those referred to the center of hydrodynamic stress, R. The position of such a center with respect to an arbitrary origin O depends on the value of the coupling tensor at O as seen in Eq. (3). García Bernal and García de la Torre[10] have shown that the coupling tensor can be evaluated in terms of the shielding coefficients

$$\Xi_{O,c} = \sum_{i=1}^{N} \zeta_i \mathbf{R}_i \times \mathbf{G}_i = \sum_{i=1}^{N} \zeta_i \mathbf{R}_i \times (\mathbf{A}_i \cdot \mathbf{G}^c_i \cdot \mathbf{A}_i) . \tag{15}$$

$\mathbf{A}_i$ in Eq. (15) is the matrix transforming Cartesian into cylindrical components, given by Eq. (I.7). $\mathbf{R}_i$ is the position vector of bead i with respect to O, and the shielding tensors in cylindrical coordinates $\mathbf{G}^c_i$ are obtained as intermediate results in the calculation of Ξ_t, as described in Paper I. If we now use Eq. (I.19) for $\mathbf{G}^c_i$, after a lengthy but simple derivation, we arrive at the final result

$$\Xi^{12}_{O,c} = \frac{1}{2} \sum_{k=1}^{N_r} \zeta_k n_k (r_k G^{rz}_k - z_k G^{\theta\theta}_k - z_k G^{rr}_k) , \tag{16}$$

with $\Xi^{21}_{O,c} = \Xi^{12}_{O,c}$, and the remaining components are zero, in agreement with the prediction of Happel and Brenner.[8] Thus, the center of hydrodynamic stress can be obtained as a by-product of the evaluation of translational coefficients.

D. Rotation around a perpendicular axis $\Xi^{22}_{R,r}$

If the particle is rotating around axis 2, which is perpendicular to the symmetry axis at an arbitrary point O, with angular velocity ω', then the unperturbed velocity of the ith bead in Cartesian coordinates is

$$\mathbf{u}_i = \omega' \times \mathbf{d}_i = \begin{pmatrix} \omega' x^3_i \\ 0 \\ \omega' x^1_i \end{pmatrix} , \tag{17}$$

where $\mathbf{d}_i = (x^1_i , 0, x^3_i)$ is the radius the ith bead with respect to axis 2. In cylindrical coordinates, $\mathbf{u}^c_i = \mathbf{A}_i \mathbf{u}_i$, so that

$$\mathbf{u}^c_i = \omega' \begin{pmatrix} -z_k \sin\theta_i \\ z_k \cos\theta_i \\ -r_k \cos\theta_i \end{pmatrix} . \tag{18}$$

We see that the components of the unperturbed velocities

of beads within a given ring are harmonic functions of θ_i. Therefore, we can suspect a similar variation for the frictional forces in cylindrical coordinates

$$F_i^\theta = E_k^\theta \sin\theta_i \ , \tag{19}$$

$$F_i^r = E_k^r \cos\theta_i \ , \tag{20}$$

$$F_i^z = E_k^z \cos\theta_i \ . \tag{21}$$

Equation (19), for instance, states that F_i^θ/u_i^θ is equal for all beads belonging to the same ring, which is to be expected owing to the symmetry of the particle. We have also confirmed Eqs. (19)–(21) in two other ways: first, by performing Jacobi iterations on Eq. (4); and second, by inspection of the numerical solution of Eq. (4) for a number of arbitrary particles.

Thus, Eqs. (19)–(21) allow a great simplification in the treatment of the hydrodynamic interaction equations. If the double sum in Eq. (4) is decomposed according to Eq. (10) and use is made of Eqs. (18)–(21), one gets after some straightforward manipulation that Eq. (4) is equivalent to

$$\sum_{l=1}^{N_r} (P_{kl}^{\theta\theta} E_l^\theta + P_{kl}^{\theta r} E_l^r + P_{kl}^{\theta z} E_l^z) = X_k^\theta \ , \tag{22}$$

$$\sum_{l=1}^{N_r} (P_{kl}^{r\theta} E_l^\theta + P_{kl}^{rr} E_l^r + P_{kl}^{rz} E_l^z) = X_k^r \ , \tag{23}$$

$$\sum_{l=1}^{N_r} (P_{kl}^{z\theta} E_l^\theta + P_{kl}^{zr} E_l^r + P_{kl}^{zz} E_l^z) = X_k^z \ , \tag{24}$$

The P_{kl}'s and X_k's are formulated in Appendix A. Thus, the original system of N linear equations, Eq. (4), is reduced to a new system, given by Eqs. (22)–(24), which has only $3N_r$ unknowns. Once Eqs. (22)–(24) are solved by direct inversion or Gauss–Siedel iterations, the frictional forces are given by Eqs. (19)–(21). Next we transform to Cartesian components by means of the A_i's, the result being

$$F_i^1 = -E_k^\theta \sin^2\theta_i + A_k^r \cos^2\theta_i \ , \tag{25}$$

$$F_i^2 = (E_k^0 + E_k^r) \sin\theta_i \cos\theta_i \ , \tag{26}$$

$$F_i^3 = E_k^z \cos\theta_i \ . \tag{27}$$

By summation of Eqs. (25)–(27) over i, we get for the total force $\mathbf{F} = (F^1, F^2, F^3)^T$, such that $F^2 = F^3 = 0$, and F^1 determines the nonzero components of the coupling tensor

$$\Xi_{O,c}^{12} = -\Xi_{O,c}^{21} = -F^1/\omega' \tag{28}$$

and

$$\Xi_{O,c}^{12} = -\sum_{k=1}^{N_r} n_k (E_k^r - E_k^\theta) \ . \tag{29}$$

It can be demonstrated that Eq. (29) is equivalent to Eq. (16).

On the other hand, Eqs. (25)–(27) can be used to obtain the individual torques from which the total torque $T = (T^1, T^2, T^3)^T$ can be obtained by summation. It turns out that $T^1 = T^3 = 0$, and the frictional coefficient for the perpendicular axes,

$$\Xi_{O,r}^{22} = T^2/\omega' = \Xi_{O,r}^{11} \tag{30}$$

is found to be

$$\Xi_{O,r}^{22} = \frac{1}{2} \sum_{k=1}^{N_r} n_k (-E_k^\theta z_k + E_k^r z_k - E_k^z r_k) \ . \tag{31}$$

E. Computational procedures

It is usual to characterize rotational dynamics in terms of diffusion coefficients. For a symmetric top macromolecule there are only two $D_r^\parallel$ and $D_r^\perp$, which correspond to the symmetry axis and to any perpendicular axis. According to Eq. (2), these are given by

$$D_r^\parallel = k_B T/\Xi_r^{33} \ , \tag{32}$$

$$D_r^\perp = k_B T/\Xi_{R,r}^{22} \ . \tag{33}$$

$D_r^\parallel$ can be obtained via Eqs. (14) and (32) from the solution of Eq. (11). As pointed out above, the location of R is not needed in this calculation. For $D_r^\perp$, however, it is necessary to find previously the position of R. As seen in Eq. (3), this requires obtaining first the Ξ_t^{11} so that the previous calculation of the translational friction tensor, or D_t, is unavoidable. Then, one would first calculate Ξ_t as described in Paper I and the coupling tensor at the arbitrary origin O by means of Eq. (16). Next, the reference axes are translated to the center of hydrodynamic stress, at which $D_r^\perp$ is calculated from Eqs. (31) and (33). Even when one is interested only in rotational results, the previous determination of D_t is useful since it is needed, for instance, in the analysis of rotational effects in quasielastic light scattering.[20,21]

F. Analytical solution for rings

The rigid ring is one of the simplest symmetric top particles. Rotational diffusion coefficients of rings with respect to both the symmetry axis $D_r^\parallel$, and a diameter $D_r^\perp$, have been obtained by Paul and Mazo[22] and Yamakawa and Yamaki[16] using the unmodified Oseen tensor. Here, we present a very simple derivation which leads to more general equations in which the finite size of the frictional elements is taken into account.

We consider a ring of radius r composed of s beads of radius σ. We have $N_r = 1$, $n_1 = s$, $r_1 = r$, and $\zeta = 6\pi\eta_0\sigma$. If the ring is rotating around the symmetry axis, the solution of Eq. (11) is $C_1 = B_{11}^{-1}$. From Eqs. (12), (14), and (32), and the expression for $T_{ij}^{\theta\theta}$ given in Eq. (I.A11) of Paper I, we get

$$D_r^\parallel = \frac{k_B T}{s\zeta r^2} \left(1 + \frac{\zeta}{8\pi\eta_0} \sum_{j\neq i}^{s} c_1 \frac{\cos\theta_j}{R_{ij}} + \frac{\zeta r^2}{8\pi\eta_0} \sum_{j\neq i}^{s} c_2 \frac{\sin^2\theta_j}{R_{ij}^3}\right) \ . \tag{34}$$

Without any loss of generality we can choose $i = s$ with $\theta_i = 2\pi$ to be used in Eq. (34). Then, $R_{sj} = 2r|\sin(\frac{1}{2}j\phi)|$ and $\theta_i = j\phi$ with $\phi = 2\pi/s$. Thus, we arrive at the final result

$$D_r^\parallel = \frac{k_B T}{6\pi\eta_0 \sigma r^2} \left(1 + \frac{3\sigma}{8r} \sum_{j=1}^{s-1} \frac{c_1 \cos j\phi}{|\sin(\frac{1}{2}j\phi)|} + \frac{3\sigma}{16r} \sum_{j=1}^{s} \frac{c_2(1+\cos j\phi)}{|\sin(\frac{1}{2}j\phi)|}\right) \ . \tag{35}$$

When the unmodified Oseen tensor is used, $c_1 = c_2 = 1$, and we recover Eq. (75) in the paper of Yamakawa and Yamaki.[16]

In a similar way we can derive an analytical solution for rotation around an axis perpendicular to that of symmetry. As the center of hydrodynamic stress is the ring's center, such an axis coincides with a diameter. For $N_r = 1$, Eqs. (22)–(24) represent a system of three linear equations that can easily be solved for E_1^θ, E_1^r, and E_1^s. All the beads in the ring have $z_i = 0$, so that

$$X_1^\theta = X_1^r = P_{11}^{\theta s} = P_{11}^{rs} = P_{11}^{s\theta} = P_{11}^{sr} = 0 \ , \tag{36}$$

and this gives

$$E_1^s = \frac{X_1^s}{P_{11}^{ss}} = -r\zeta\omega' \Big(\cos\theta_1 + \zeta(8\pi\eta_0)^{-1} \times \sum_{j\neq 1}^{s} c_1 \cos\theta_j R_{1j}^{-1} \Big)^{-1} \ . \tag{37}$$

If we now take $i = s$ and $\theta_i = 2\pi$ as before, the use of Eqs. (31) and (33) leads to

$$D_r^\perp = \frac{k_B T}{3\pi\eta_0 \sigma s r^2} \times \Big(1 + \frac{3\sigma}{4r} \sum_{j=1}^{s-1} \frac{c_1 \cos j\phi}{|\sin(\frac{1}{2} j\phi)|} \Big) \ . \tag{38}$$

It can be shown that in the case of the unmodified tensor, Eq. (38) reduces to Eq. (80) in the paper by Yamakawa and Yamaki.[16]

G. An approximate method

A further reduction in the computational effort needed to get the rotational coefficients can be achieved by making approximations in the formalism we have presented so far. Some alternatives in this direction are presented here.

Let us now define a new system of cylindrical coordinates whose axial, radial and angular coordinates are denoted, respectively, as t, ρ, and ϕ in such a way that t is measured along the rotation (not the particle's) axis. Following Yamakawa and Yamaki,[16] we adopt the simplifying assumption that the frictional force at element i is proportional to its unperturbed linear velocity $\mathbf{u}_i$, and define a factor H_i by means of

$$\mathbf{F}_i = \zeta_i H_i \mathbf{u}_i \ , \tag{39}$$

where $\mathbf{u}_i = (\omega^t \rho_i, 0, 0)$. If t is the symmetry axis or any axis perpendicular to it, one can show that $H_i = H_k$ for all the elements belonging to ring k. This tell us that the present problem is completely similar to that solved for rotation around the symmetry axis. Then, following the same steps as in Sec. II.B we arrive at the result

$$\Xi_r^t = \sum_{k=1}^{N_r} n_k H_k (\rho_k)^2 \zeta_k \ , \tag{40}$$

where the H_k's are the N_r unknowns of the set of linear equations

$$\sum_{k=1}^{N_r} J_{kl} H_l = 1 \ ,$$

whose coefficients are given by

$$J_{kl} = \delta_{kl} \Big(1 + \sum_{j\in k}{}' \zeta_j T_{ij}^{\phi\phi} \Big) + (1 - \delta_{kl}) r_k r_l^{-1} \sum_{j\in l} \zeta_j T_{ij}^{\phi\phi} \ . \tag{41}$$

$T_{ij}^{\phi\phi}$ is the diagonal angular component of the interaction tensor given by Eq. (I.A1) of Paper I with ϕ in place of θ.

For rotation around the symmetry axis, Eq. (39) is not an approximation but an exact relationship. Equations (39)–(41) reduce to (5), (6), (11), and (14) with $H_k \equiv C_k$, $J_{kl} \equiv B_{kl}$, $\rho_i \equiv r_i$, and $\Xi_r^t \equiv \Xi_{rr}^{33}$. Let us now consider the rotation around any perpendicular axis, such as x^2. If we look at E$_\perp$s. (17) and (25)–(27) and consider that $x_i^3 = z_i$, $x_i^1 = r_i \cos\theta_i$, we then find that the necessary and sufficient conditions for Eq. (39) to hold are

$$E_k^\theta = -E_k^r \tag{42}$$

and

$$E_k^\theta / E_k^s = z_k / r_k \ . \tag{43}$$

Equations (42) and (43) are simultaneously satisfied only in some particular cases. Thus, for a ring, it follows from Eq. (36) that $E_1^\theta = -E_1^r = 0$ and $E_1^\theta / E_1^s = 0 = z_1 / r$. Also, for any linear structure (recall that a bead on the symmetry axis can be regarded as a ring with $n_k = 1$ and $r_k = 0$) it can be straightforwardly demonstrated that $E_k^\theta = -E_r^r$ and $E_k^s = 0$, so that Eq. (43) is satisfied as well.

In previous works by Bloomfield and co-workers[12–15] the approximate method discussed here was applied to the calculation of rotational diffusion coefficients of ellipsoidal models, lollipops, dumbbells, and T-even bacteriophage. Except in the latter case the approximation is exact because the models are linear. For the bacteriophage models (see Fig. 1 in Ref. 13) we have now recalculated $D_r^\perp$ by the exact procedure. The resulting values differ from those reported previously only by 2% for the slow forms and 5% for the fast forms. The good performance of the approximate method is surely due to the fact that the bacteriophage head and tail, which account for a large portion of the rotational friction, are modeled by collinear beads lying on the symmetry axis that therefore obey Eqs. (42) and (43).

III. APPLICATION TO CYLINDERS

A. Rotation around a perpendicular axis

As in Paper I, right circular cylinders were modeled by stacking N_r rings, each composed of s touching beads of radius σ. Two stacking modes were considered. In mode A, the beads are vertically aligned, while in mode B each ring is rotated π/s to get closest packing. The surface element density[1] λ is a function of s and depends on the stacking mode. The calculations were carried out for $s = 6$, 8, 12, 16, and 25 in mode A and $s = 6$ and 12 in mode B. The radius R and length L of the cylinder are taken as the circumscribed radius and the total length of the model, respectively. Since cylinders have an additional plane of symmetry perpendicular to the axis, no translation–rotation coupling occurs, and the center of hydrodynamic stress is just the particle center.

TABLE I. Values of $\delta_\perp(\infty, \lambda)$, $f(\lambda)$, and $g(\lambda)$ in Eq. (46).

s	Mode	$\delta(\infty, \lambda)$	$e(\lambda)$	$f(\lambda)$
6	A	−0.425	0.762	0.077
8	A	−0.456	0.698	0.204
12	A	−0.505	0.705	0.178
16	A	−0.538	0.743	0.139
25	A	−0.582	0.797	0.095
6	B	−0.432	0.804	0.021
12	B	−0.510	0.757	0.089

The variation of the rotational friction and diffusion coefficients for rotation around a perpendicular axis can be formulated as

$$\frac{\pi\eta_0 L^3}{3\Xi^{22}} = \frac{\pi\eta_0 L^3 D_r^\perp}{3k_B T} = \ln p + \delta_\perp , \tag{44}$$

where $p = L/2R$ is the length-to-diameter ratio. $\delta_\perp$ is the end-effect correction, that depends on p and, for our models made of discrete elements, on λ as well. According to the Oseen–Burgers calculations by Yamakawa,[23] $\delta_\perp$ can be expressed as a power expansion in p^{-1}. As we will show later, a second-degree polynomial gives an excellent reproduction of the observed behavior of $\delta_\perp(p, \lambda)$ for all the models when $p > 2$, so that we retain only the three leading terms

$$\delta_\perp(p, \lambda) = \delta_\perp(\infty, \lambda) + e(\lambda)p^{-1} + f(\lambda)p^{-2} . \tag{45}$$

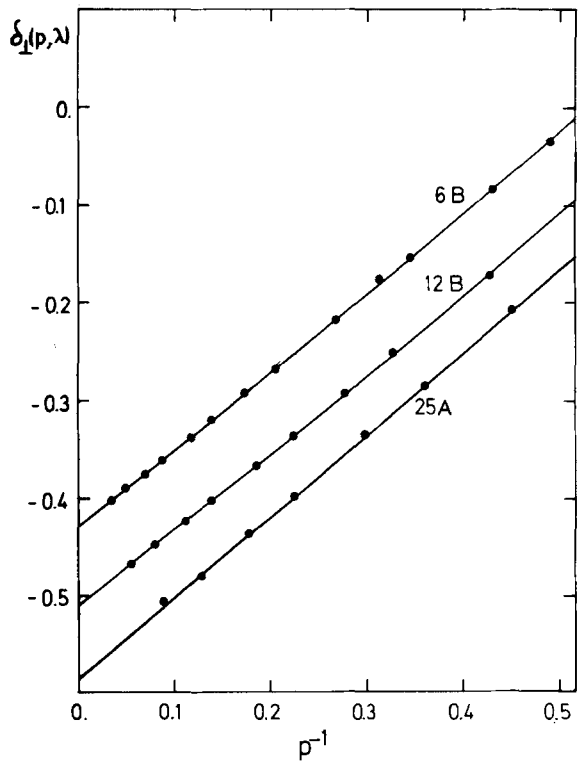

FIG. 1. Values of $\delta_\perp$ plotted vs p^{-1} for three different models. The number and letter attached to each curve stand, respectively, for the corresponding value of s and the stacking mode. Dots are results calculated from Eqs. (31), (33), and (44), and the continuous lines are the least-squares quadratic functions used for interpretation.

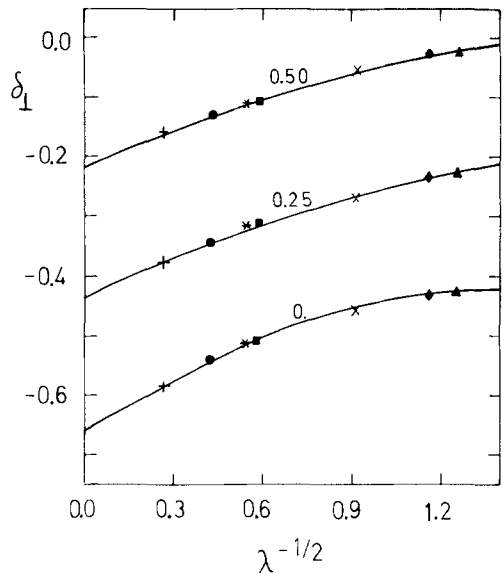

FIG. 2. Quadratic extrapolation to the $\lambda \to \infty$ limit of results for the several cylindrical models with different λ and constant p. The numbers attached to the curves are the values of p^{-1}. Notation for the data points is as follows: (▲) $s = 6$, mode A; (◆) $s = 6$, mode B; (×) $s = 8$, mode A; (■) $s = 12$, mode A; (*) $s = 12$, mode B; (●) $s = 16$, mode A; (+) $s = 25$, mode A. The solid lines are the least-squares second-degree polynomials, Eq. (45).

For each s and stacking mode, and varying N_r up to 100, we have calculated numerically $\delta_\perp(p, \lambda)$ from Eqs. (31), (33), and (44). The coefficients $\delta_\perp(\infty, \lambda)$, $e(\lambda)$, and $g(\lambda)$ were obtained for each s and mode by least-squares fitting. An excellent linearity was found in all cases, and some examples of this are displayed in Fig. 1. The resulting values of $\delta_\perp(\infty, \lambda)$ and $e(\lambda)$ are listed in Table I. Next, Eq. (44) was used to interpolate $\delta_\perp(p, \lambda)$ at fixed values of p for each model and s. Then we extrapolated the $\delta_\perp(p, \lambda)$ for a fixed p and varying λ to $\lambda \to \infty$ by obtaining the intercept at $\lambda^{-1/2} = 0$ in $\delta_\perp(p, \delta)$ vs $\lambda^{-1/2}$ plots as we did in Paper I. Now the curves were not linear but they showed a noticeable downwards curvature, as evidenced for some values of p^{-1} in Fig. 2. Therefore, $\delta_\perp(p, \infty)$ had to be obtained by means of quadratic extrapolation

TABLE II. End-effect corrections $\delta_\perp$ and $\delta_\parallel$, calculated by extrapolation to $\lambda \to \infty$ of results for cylindrical models.

p^{-1}	$\delta_\perp$	$\delta_\parallel$
0.50	−0.216	0.294
0.45	−0.260	0.269
0.40	−0.303	0.243
0.35	−0.348	0.216
0.30	−0.392	0.189
0.25	−0.436	0.159
0.20	−0.481	0.130
0.15	−0.526	0.099
0.10	−0.571	0.067
0.05	−0.616	0.034
0	−0.662	0

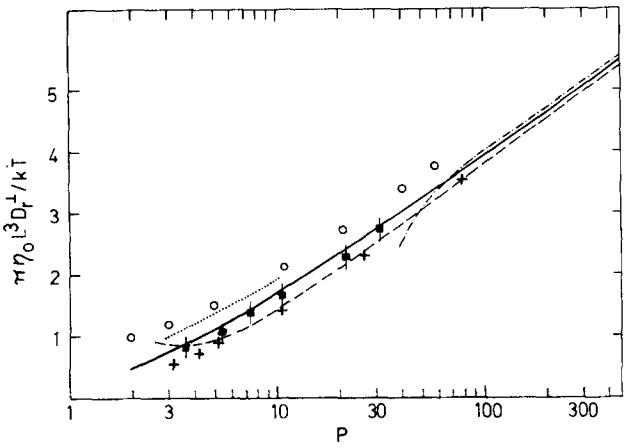

FIG. 3. Semilogarithmic plot of the rotational diffusion coefficient, normalized as indicated, against p: (■) Experimental results by Broersma (Ref. 19) with indication of the estimated errors as vertical bars; (----) Borersma's semiempirical equation (47); (+) Broersma's theoretical results taken from Table I in Ref. 19; (- •- •-) Yamakawa's equation (48); (• • •) results from the hydrodynamically rigorous calculation by Yoshizaki and Yamakawa (Ref. 24); (o) results for a rod of touching spheres obtained by Nakajima and Wada (Ref. 3); (—) this work.

$$\delta_\perp(p, \lambda) = \delta_\perp(p, \infty) + g(p)\lambda^{-1/2} + h(p)(\lambda^{-1/2})^2 , \qquad (46)$$

whose coefficients were calculated by least-squares fits. The $\delta_\perp(p, \infty)$ are summarized in Table II, and, when substituted into Eq. (44) they lead to the rotational diffusion coefficients that are plotted against $\ln p$ as a continuous line in Fig. 3. Our value for the end-effect correction in the $p \to \infty$ limit is $\delta_\perp(\infty, \infty) = -0.662$.

The first calculation of the rotational coefficients of finite cylinders was that by Broersma[19] whose results have been used extensively during the past twenty years to get the cylinder dimensions from the experimentally observed diffusion coefficient. Broersma made a theoretical calculation of $D_r^\perp$ for varying p whose results are represented by crosses in Fig. 3. His value for the end-effect correction of infinitely long cylinders is $\delta_\perp(\infty, \infty) = -0.447$. He also made experimental measurements on macroscopic cylinders, that are also included in Fig. 3. Finally, Broersma obtained a semiempirical equation that fits predominantly the experimental results at low p and the theoretical values at high p. His equation is

$$\delta_\perp = -0.88 + 7[(\ln 2p)^{-1} - 0.28]^2 . \qquad (47)$$

The problem was later reconsidered by Yamakawa and Yoshizaki.[23,24] First, Yamakawa[23] made a Oseen–Burgers-type numerical calculation of the end-effect correction, arriving at the expression

$$\delta_\perp = -0.481312 - 38.9683p^{-1} + 3691.64p^{-2} - 128.672p^{-3} , \qquad (48)$$

which was supposed to be correct within 1% for $p > 60$. The results from Eqs. (48) and (44) have also been included in Fig. 3. In addition, he obtained the same value as Broersma[19] in an analytical evaluation at the $p \to \infty$ limit. More recently Yoshizaki and Yamakawa[24] have determined the rotational coefficient of cylinders capped with hemispheroids at the ends by the use of an orthodox method of classical hydrodynamics and showed that Eq. (48) is in agreement with the exact values when $p > 60$. For low p, they reported results obtained by solving numerically their hydrodynamic integral equations for different sizes of the caps, but they reported no values for uncapped cylinders like those studied in this paper. Nonetheless Yoshizaki and Yamakawa have proved that the terminal effects from the caps on the translational and rotational coefficients are negligible for $p > 3$ in accordance with previous works.[1,18] Therefore, we have assumed that the values reported in Fig. 3 of their paper,[24] covering the range $3 < p < 10$, are those their theory would give for uncapped short cylinders. These values are plotted, after a change of ordinate, in our Fig. 3.

Finally, we have also plotted in Fig. 3 as open circles the results for a rod composed of colinear touching spheres as calculated by Nakajima and Wada,[3] so that the differences between cylindrical and noncylindrical models can be seen.

In the analysis of the results displayed in Fig. 3 it is convenient to distinguish two regions, one for short cylinders with p lesser than, say, 30, and other corresponding to long cylinders. In the region of low p, it is tempting to compare the experimental points obtained by Broersma[19] with the several theoretical predictions. As seen in Fig. 3 such comparison is most favorable for the results calculated in this paper, while the values of Broersma and Yoshizaki and Yamakawa[24] are noticeably lower and higher, respectively, than the experimental ones. The curve corresponding to our results is even closer to the experimental data than the semiempirical equation of Broersma,[19] in which those points were taken into account. These conclusions, however, must be taken with caution. First because our results could be a little biased owing to unknown effects in the extrapolation to $\lambda \to \infty$. And second, because the experimental data could be vitiated by wall effects from the container in which measurements were done, as pointed out by Broersma himself.

All the previous calculations gave $\delta_\perp = -0.447$ for an infinitely long cylinder, while our result is $\delta_\perp = -0.662$. The discrepancy is surely due to the inadequacy of Eq. (45) with regard to its use for extrapolating at $p \to \infty$. Indeed, results for models with $s = 3$ and $s = 1$ (rod of touching beads) that can reach a higher p for the maximum N_r showed a nearly flat region in the $\delta_\perp(p, \lambda)$ vs p^{-1} plot in the vicinity of $p^{-1} = 0$ and there could be even a minimum followed by an ascending final portion of the curve. Such a trend is actually observed in the case of the end-effect correction for translational motion γ, as calculated by Youngren and Acrivos[25] (see Fig. 3 in Paper I).

It should be remarked that the $p \to \infty$ limit is physically unattainable. All the macromolecules on could model as rigid straight cylinders, such as TMV and short pieces of DNA and polypeptides, certainly have length-to-diameter ratios $p = 30$–300, within the high p region of Fig. 3.

When $p = 200$, for instance, $\delta_\perp$(Yamakawa) = − 0.60, $\delta_\perp$(Broersma) = − 0.74, and our calculation yields $\delta_\perp$ = − 0.65, an intermediate value that is closer to them than in the $p \to \infty$ case. The discrepancies between the three theories probably comes from the physical or numerical approximations embodied in all of them. Fortunately, the contribution of $\delta_\perp$ becames less and less important as p increases, and the differences in the calculated diffusion coefficients with the three different $\delta_\perp$'s fall well within typical instrumental errors.

To end this discussion, we would like to point out that when the axial ratio is not too large, the touching spheres model of a rod deviates remarkably from all the theoretical prediction for cylinders, as is evident from Fig. 3. Rodlike bipolymers usually have an uniform cross-section so that the cylindrical representation is most adequate, and our analysis shows that the touching spheres rod can lead to an important overestimation of the rotational diffusion coefficient.

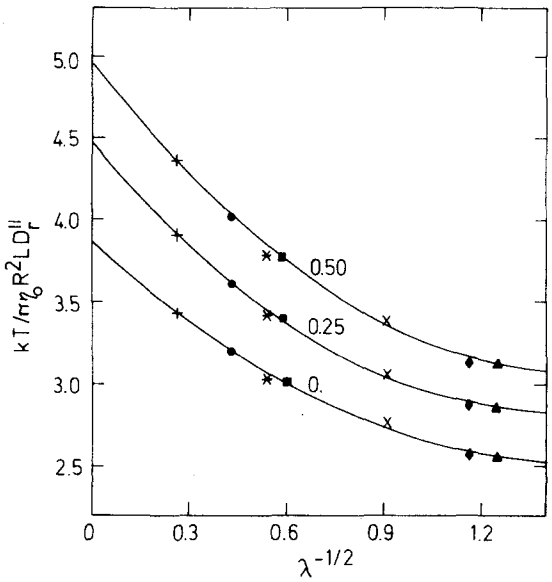

FIG. 5. Same as in Fig. 2 for rotation around the symmetry axis.

B. Rotation around the symmetry axis

As this case can not be treated by the Oseen–Burgers procedure, no previous theoretical studies are available, except the recent one by Yoshizaki and Yamakawa[24] which deals only with short length-to-diameter ratio. The analytical results of Perrin[25,26] for Ξ_r^{33} (or $kT/D_r^{\parallel}$) of prolate ellipsoids when plotted as $k_B T/\pi\eta_0 L R^2 D_r^{\parallel}$ vs p^{-1} give a line with little curvature. We assume that the same dependence holds for cylinders, so that a quadratic function in p^{-1} can be used for intrapolation and extrapolation

$$k_B T/\pi\eta_0 L R^2 D_r^{\parallel} = A_0 + A_1 p^{-1} + A_2 p^{-2} . \tag{49}$$

As it is seen Fig. 4 for a few models, the least-squares second-degree polynomials fit rather well the numerical results. For each model the A_0, A_1, and A_2 obtained by the least-squares method were used to calculate the term on the right-hand side of Eq. (49) for fixed values of p^{-1}. The interpolated values were then extrapolated to the $\lambda \to 0$ limit using second-degree polynomials like those in Eq. (46). Some examples of the extrapolation are shown in Fig. 5. The resulting values have been plotted versus p^{-1} in Fig. 4 as a thick curve.

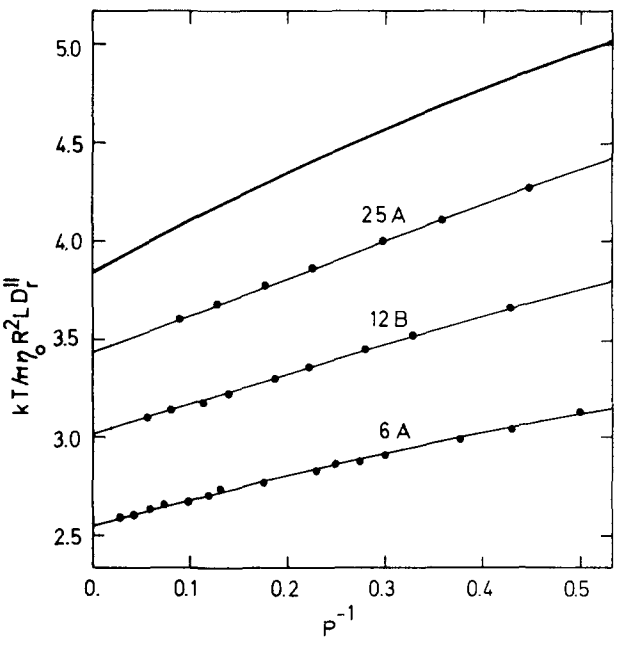

FIG. 4. Values of the rotational diffusion coefficient for rotation around the symmetry axis, expressed as $kT/\pi\eta_0 R^2 L D_r^{\parallel}$), plotted vs p^{-1}. Dots are results from Eqs. (11), (14), and (32) for three types of cylindrical models that are denoted as in Fig. 1. Thin lines are the least-squares quadratic curves used for interpolation and extrapolation, as formulated in Eq. (49). The thick unlabeled curve represents the results for a perfect cylinder after extrapolation to infinite surface element density (Fig. 5).

As in the previous case, an end-effect correction $\delta_{\parallel}$ can be used to characterize finite cylinders. A suitable definition for $\delta_{\parallel}$ is

$$k_B T/A_0 \pi\eta_0 L R^2 D_r^{\parallel} = 1 + \delta_{\parallel} , \tag{50}$$

where $A_0 = 3.841$ as obtained from the $\lambda \to \infty$ extrapolation of data for $p^{-1} = 0$. $\delta_{\parallel}$ is presented as a function of p^{-1} in Table I.

It should be noted that in many cases of interest the rotation around the symmetry axis of a symmetric top macromolecule is not observed experimentally, for the principal directions of the electro-optical properties usually coincide with the rotational axes. This is in contrast with the fact that $D_r^{\parallel}$ is much more sensitive to the cylinder's cross section than $D_r^{\perp}$ and the translational diffusion coefficient are. Therefore, $D_r^{\parallel}$ provides a potentially useful way to determine precisely the radius of rodlike macromolecules, for which the other properties give estimates that can be highly biased by uncertainties in the end-effect corrections. For instance, if a suitable chromophore could be attached in such a way that the absorbing and emitting dipoles make an angle with the symmetry axis, $D_r^{\parallel}$ would be accessible from the fluorescence anisotropy decay curve.[27]

APPENDIX A

The P_{kl}'s and X_k's in Eqs. (22)–(24) are given by

$$P_{kl}^{\theta\theta} = (1-\delta_{kl})\left(\sin\theta_i + \zeta_k \sum_{j\in k}{}' T_{ij}^{\theta\theta}\sin\theta_j\right) + \delta_{kl}\zeta_k \sum_{j\in l} T_{ij}^{\theta\theta}\sin\theta_j \,, \tag{A1}$$

$$P_{kl}^{\theta r} = (1-\delta_{kl})\zeta_k \sum_{j\in k}{}' T_{ij}^{\theta r}\cos\theta_j + \delta_{kl}\zeta_k \sum_{j\in k} T_{ij}^{\theta r}\cos\theta_j \,, \tag{A2}$$

$$P_{kl}^{\theta z} = (1-\delta_{kl})\zeta_k \sum_{j\in k}{}' T_{ij}^{\theta z}\cos\theta_j + \delta_{kl}\zeta_k \sum_{j\in l} T_{ij}^{\theta z}\cos\theta_j \,, \tag{A3}$$

$$P_{kl}^{r\theta} = (1-\delta_{kl})\zeta_k \sum_{j\in k}{}' T_{ij}^{r\theta}\sin\theta_j + \delta_{kl}\zeta_k \sum_{j\in l} T_{ij}^{r\theta}\sin\theta_j \,, \tag{A4}$$

$$P_{kl}^{rr} = (1-\delta_{kl})\left(\cos\theta_i + \zeta_k \sum_{j\in k}{}' T_{ij}^{rr}\cos\theta_j\right) + \delta_{kl}\zeta_k \sum_{j\in l} T_{ij}^{rr}\cos\theta_j \,, \tag{A5}$$

$$P_{kl}^{rz} = (1-\delta_{kl})\zeta_k \sum_{j\in k}{}' T_{ij}^{rz}\cos\theta_j + \delta_{kl}\zeta_k \sum_{j\in l} T_{ij}^{rz}\cos\theta_j \,, \tag{A6}$$

$$P_{kl}^{z\theta} = (1-\delta_{kl})\zeta_k \sum_{j\in k}{}' T_{ij}^{z\theta}\sin\theta_j + \delta_{kl}\zeta_k \sum_{j\in l} T_{ij}^{z\theta}\sin\theta_j \,, \tag{A7}$$

$$P_{kl}^{zr} = (1-\delta_{kl})\zeta_k \sum_{j\in k}{}' T_{ij}^{zr}\cos\theta_j + \delta_{kl}\zeta_k \sum_{j\in l} T_{ij}^{zr}\cos\theta_j \,, \tag{A8}$$

$$P_{kl}^{zz} = (1-\delta_{kl})\left(\cos\theta_i + \zeta_k \sum_{j\in k}{}' T_{ij}^{zz}\cos\theta_j\right) + \delta_{kl}\zeta_k \sum_{j\in l} T_{ij}^{zz}\cos\theta_j \,, \tag{A9}$$

and

$$X_k^{\theta} = -z_k \sin\theta_i \zeta_k \omega^2 \,, \tag{A10}$$

$$X_k^{r} = z_k \cos\theta_i \zeta_k \omega^2 \,, \tag{A11}$$

$$X_k^{z} = -r_k \cos\theta_i \zeta_k \omega^2 \,. \tag{A12}$$

In Eqs. (A1)–(A11), i is an arbitrary bead belonging to the kth ring. The results for the E_k's do not depend on the choice of i. The summation $\sum'_{j\in k}$ is extended to all beads in ring k except bead i. The summation $\sum_{j\in l}$ is extended to all the beads in ring l. δ_{kl} is Kronecker's delta.

A single bead on the symmetry axis must be considered as a ring with $n_k = 1$, $r_k = 0$, and $\theta_i = 0$.

[1] M. M. Tirado and J. García de la Torre, J. Chem. Phys. 71, 2581 (1979).
[2] J. A. McCammon and J. M. Deutch, Biopolymers 15, 1397 (1976).
[3] H. Nakajima and Y. Wada, Biopolymers 16, 875 (1977).
[4] J. García de la Torre and V. A. Bloomfield, Biopolymers 16, 1747 (1977).
[5] J. García de la Torre and V. A. Bloomfield, Biopolymers 17, 1605 (1978).
[6] E. Swanson, D. C. Teller, and C. de Haen, J. Chem. Phys. 68, 5097 (1978).
[7] V. A. Bloomfield, W. O. Dalton, and K. E. Van Holde, Biopolymers 5, 135 (1967).
[8] J. Happel and H. Brenner, *Low Reynolds Number Hydrodynamics* (Nordhoff, Leyden, 1973), Chap. 5.
[9] H. Brenner, J. Colloid Interface Sci. 23, 407 (1967).
[10] J. M. García Bernal and J. García de la Torre, Biopolymers (to be published).
[11] S. Harvey and J. García de la Torre, Macromolecules (to be published).
[12] J. García de la Torre and V. A. Bloomfield, Biopolymers 16, 1765 (1977).
[13] J. García de la Torre and V. A. Bloomfield, Biopolymers 16, 1779 (1977).
[14] R. W. Wilson and V. A. Bloomfield, Biopolymers 18, 1205 (1979).
[15] V. A. Bloomfield, J. García de la Torre, and R. W. Wilson, in *Electro-optics and Dielectrics of Macromolecules and Colloids*, edited by B. R. Jennings (Plenum, New York, 1979), p. 183.
[16] H. Yamakawa and J. Yamaki, J. Chem. Phys. 58, 2049 (1973).
[17] S. Broersma, J. Chem. Phys. 32, 1632 (1960).
[18] T. Norisuye, M. Motokawa, and H. Fijita, Macromolecules 12, 320 (1979).
[19] S. Broersma, J. Chem. Phys. 32, 1626 (1960).
[20] R. W. Wilson and V. A. Bloomfield, Biopolymers 18, 1543 (1979).
[21] G. Koopmans, B. J. van der Meer, P. C. Hopman, and J. Greve, Biopolymers 18, 1533 (1979).
[22] E. Paul and R. M. Mazo, J. Chem. Phys. 48, 2378 (1968).
[23] H. Yamakawa, Macromolecules 8, 339 (1975).
[24] T. Yoshizaki and H. Yamakawa, J. Chem. Phys. 72, 57 (1980).
[25] F. Perrin, J. Phys. Radium 7, 1 (1936).
[26] S. Koening, Biopolymers 14, 2421 (1975).
[27] G. G. Belford, R. L. Belford, and G. Weber, Proc. Natl. Acad. Sci. U. S. A. 69, 1392 (1972).